

Article

Realizing Dual Functions through Y_2O_3 Modification to Enhance the Electrochemical Performance of $LiNi_{0.8}Co_{0.1}Mn_{0.1}O_2$ Material

Xintao Wang , Feng Wang *, Meiqi Zheng, Maohua Rong , Jiang Wang *, Jianqiu Deng , Peng Liu and Daosheng Liu

School of Materials Science and Engineering & Guangxi Key Laboratory of Information Materials, Guilin University of Electronic Technology, Guilin 541004, China; jqdeng@guet.edu.cn (J.D.)

* Correspondence: wf@guet.edu.cn (F.W.); waj124@guet.edu.cn (J.W.)

Abstract: In recent years, the remarkable energy density of high-nickel ternary materials has captured considerable attention. Nevertheless, the high-nickel ternary cathode material encounters several challenges, including cationic mixing, microcrack formation, poor cycling capability, and limited thermal stability. Coating, as a viable approach, proves to be effective in enhancing the material properties. In this study, the $LiNi_{0.8}Co_{0.1}Mn_{0.1}O_2$ (NCM811) sample underwent a dry grinding process, followed by Y_2O_3 coating and subsequent sintering at varying temperatures. The microstructure, morphology, and electrochemical properties of the materials were meticulously examined, and the underlying mechanism of coating modification was meticulously explored. The outcomes demonstrate the attainment of dual coating and doping effects through Y_2O_3 modification. Y_2O_3 coating mitigates the direct interaction between the NCM811 surface and the electrolyte, thereby inhibiting undesired side reactions at the interface. Moreover, the Y element infiltrates the crystal structure, imparting stability at elevated sintering temperatures. Remarkably, the Y_2O_3 -coated cathode materials exhibit significantly enhanced cycling stability, discharge capacity, and rate performance. These findings can provide novel insights that can be harnessed to improve the energy density cathode material of NCM811.

Keywords: lithium-ion battery; $LiNi_{0.8}Co_{0.1}Mn_{0.1}O_2$ cathode material; Y_2O_3 modification; dual functions; cycle stability



Citation: Wang, X.; Wang, F.; Zheng, M.; Rong, M.; Wang, J.; Deng, J.; Liu, P.; Liu, D. Realizing Dual Functions through Y_2O_3 Modification to Enhance the Electrochemical Performance of $LiNi_{0.8}Co_{0.1}Mn_{0.1}O_2$ Material. *Coatings* **2024**, *14*, 443. <https://doi.org/10.3390/coatings14040443>

Academic Editors: Gergana Alexieva, Rositsa Gergova and Tsvetanka Babeva

Received: 14 March 2024

Revised: 3 April 2024

Accepted: 4 April 2024

Published: 8 April 2024



Copyright: © 2024 by the authors. Licensee MDPI, Basel, Switzerland. This article is an open access article distributed under the terms and conditions of the Creative Commons Attribution (CC BY) license (<https://creativecommons.org/licenses/by/4.0/>).

1. Introduction

Long range is the primary technical index of new energy vehicles. Under the premise of ensuring safety, it is an inevitable development trend to continuously improve the energy density of batteries [1,2]. The cathode material is one of the decisive factors that determine the energy density of lithium-ion batteries. Layered transition metal oxides for lithium-ion batteries have the advantages of high energy density, good cycle stability, and rapid charge and discharge [3]. The earliest $LiCoO_2$ materials have relatively low capacity, and Co is expensive, highly toxic, and scarce [4]. $LiNiO_2$ is prone to thermal runaway reactions during overcharge and overdischarge. $LiMnO_2$ is prone to short cycle life and capacity decay at high temperatures. The ternary high-nickel cathode materials have the advantages of low cost, good safety performance, and high capacity. To a certain extent, the advantages of various cathode materials are comprehensively used to improve the performance and stability of batteries. The increase in nickel content is helpful to increase the capacity of the battery. However, Ni^{2+} and Li^+ easily switch positions, which adversely affects its cycle performance, because the radius of Li^+ is very close to that of Ni^{2+} . High-nickel materials are also prone to react with H_2O and CO_2 in the air to produce $LiOH$ and Li_2CO_3 , which can cause side reactions with electrolytes and lead to surface instability [5]. In addition, lattice oxygen precipitation, microcrack formation, and other problems lead to the destruction of its structure and capacity attenuation.

According to the characteristics of high-nickel materials, coating and doping methods are generally used to improve their properties. The commonly used coating materials are phosphates, fluorides, metal oxides, etc., such as Al_2O_3 [6–8], MgO [9,10], CeO_2 [11], TiO_2 [12], AlPO_4 [6,13], AlF_3 [14], CaF_2 [15], LiF [16], etc. Fluoride coating has strong corrosion resistance and effectively protects the performance of high-nickel materials in corrosive media [17–19]. However, it is easy to fail in a high-temperature reduction environment; the coating layer is relatively brittle and easy to crack or peel, which affects the stability and protection effect of the coating layer [20]. Phosphate coating has good electrochemical properties, but its structural stability is poor, and it is prone to phase transition or reaction to form precipitation, which affects the stability and protection effect of coating [21–23]. The metal oxide coating can isolate the cathode material from the electrolyte and minimize the harmful side reactions, thus protecting the surface of the material from the erosion of the electrolyte during charge and discharge [21,24]. As a rare earth element, yttrium has high oxygen affinity. At the same time, yttrium oxide (Y_2O_3) has excellent chemical inertia, high corrosion resistance, outstanding thermal stability, promoted electron transfer, and so on [25]. Liu et al. reported that coating $\text{LiNi}_{0.5}\text{Co}_{0.2}\text{Mn}_{0.3}\text{O}_2$ with yttrium oxide can successfully improve its cycle and rate performance and reduce the internal resistance of the material [26]. Therefore, using yttrium oxide coating in a high-nickel cathode material system will be a beneficial attempt.

Among the various coating methods, wet coating is widely used. The existence of media such as water may lead to lithium leaching and a change in positive electrode surface stoichiometry [27,28]. ALD coating is a method of depositing material layer by layer through gas phase reaction, but the process is complex, slow, and it requires highly precise control [29]. CVD is formed by sending gaseous reactants into the reaction chamber to form a coating on the surface of the substrate [30]. This coating process requires vacuum conditions and high temperatures, and the equipment cost is high [31]. Dry coating does not require a liquid phase medium and the process is relatively simple. It is a method that can achieve high-speed and efficient production and is suitable for large-scale preparation. In order to better meet the needs of practical production, this study adopts Y_2O_3 coating via the dry milling method to prepare $\text{LiNi}_{0.8}\text{Co}_{0.1}\text{Mn}_{0.1}\text{O}_2$ cathode material and investigates the effect of Y_2O_3 modification on the cathode material at different sintering temperatures. Y_2O_3 can improve the electrochemical performance of lithium-ion batteries through the synergistic improvement of coating and doping at higher temperatures.

2. Materials and Methods

2.1. Materials Preparation

The materials and reagents used in this experiment are commercial materials. Nano-scale Y_2O_3 powder was purchased from the Shanghai Pacific Technology limited company. $\text{LiNi}_{0.8}\text{Co}_{0.1}\text{Mn}_{0.1}\text{O}_2$ powder was purchased from the Dongguan Oriental Sunshine Scientific Research and Development limited company. $\text{LiNi}_{0.8}\text{Co}_{0.1}\text{Mn}_{0.1}\text{O}_2$ was taken as the coated object, and Y_2O_3 was taken as the coating material. A total of 0.5 g of $\text{LiNi}_{0.8}\text{Co}_{0.1}\text{Mn}_{0.1}\text{O}_2$ and 0.01 g (coating amount is 2 wt %) of Y_2O_3 were weighed into an agate mortar and fully milled. The target samples were obtained via calcination at different temperatures (400 °C, 700 °C, and 750 °C) for 12 h. The samples were labeled NCM@YO400, NCM@YO700, and NCM@YO750, respectively. The sample and the assembled button battery used for synthesis in this experiment are shown in Figures S1 and S2.

2.2. Material Characterization

The material characterization methods used in this experiment are X-ray diffraction (XRD, Rigaku D/max2550 VB, Showima City, Tokyo, Japan), scanning electron microscopy (SEM, Quanta 450 FEG, FEI, Hillsboro, OR, USA), energy-dispersive X-ray detection (EDX), high-resolution transmission electron microscopy (HRTEM, Hillsborough, OR, USA), and X-ray photoelectron spectroscopy (XPS, ESCALAB250xi, Waltham, MA, USA). The spe-

cific parameters used can be found in the literature previously reported by our research group [32]. The XRD data was analyzed using JADE software (JADE 9).

2.3. Electrochemical Measurement

The electrochemical performance of the Land CT2001A battery testing system (1 C = 200 mA g⁻¹) was tested at room temperature in the voltage range of 2.8–4.3 V and 2.8–4.5 V, respectively. The scanning speed of the cyclic voltammetry curve was 0.1 mV S⁻¹, and the scanning range was 2.8 V–4.5 V (relative to Li/Li⁺). In the amplitude of 5 mV and the frequency range of 0.01 Hz~100 KHz, the electrochemical impedance spectroscopy (EIS) test was performed. EIS curves of 150 cycles were obtained.

3. Results

The XRD spectrum and amplification spectrum of pure NCM811 and Y₂O₃-coated NCM811 samples belong to the R3m space group as shown in Figure 1a, which is a hexagonal lamellar structure of α -NaFeO₂. The pure NCM811 is consistent with PDF standard card #87-1562. At the same time, sharp visible peaks are observed at $2\theta \approx 29.15^\circ$ and $2\theta \approx 33.79^\circ$ of the Y₂O₃-modified NCM811 sample, which is consistent with PDF card #791257 through analysis and belongs to the Ia-3 space group. The (108)/(110) and (006)/(102) peaks split obviously, indicating that pure NCM811 and Y₂O₃-modified NCM811 maintain a highly ordered layered hexagonal structure [33]. The Rietveld refinement parameters of bare and Y₂O₃-modified NCM811 samples are shown in (Figure 1b) and Table 1. The strength ratios of I₍₀₀₃₎/I₍₀₀₄₎ of the samples are 1.5066, 1.5506, 1.5124, and 1.5263, respectively, which are much higher than 1.20, confirming the low cation ordered layer structure mixing. The amplification of the doped (003) peak shifts to smaller angles, and the shifted angles are 0.04° (NCM811@YO400), 0.08° (NCM811@YO700), and 0.10° (NCM811@YO750), respectively. The above results may be due to the fact that the ion radius of Y³⁺ is larger than that of transition metal ions M (M=Ni, Co, Mn), and some Y is doped into NCM811 materials, which increases the host cell parameters and enlarges the plane spacing of the materials. Increasing the plane spacing can effectively improve the diffusion rate of Li⁺ [34].

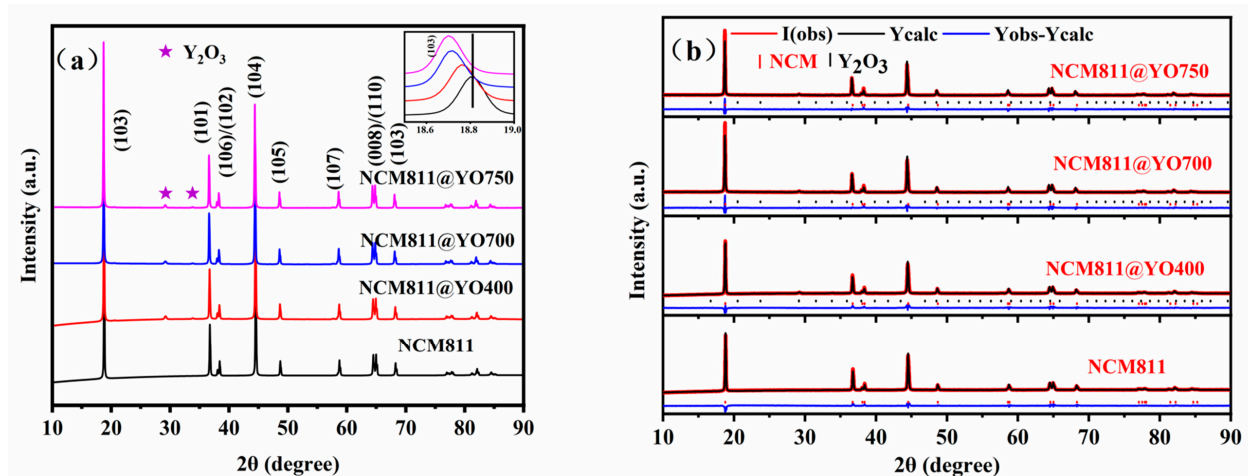


Figure 1. (a) XRD patterns of pure NCM811 and Y₂O₃-modified NCM811 samples. (b) Patterns of the Rietveld refinement parameter for NCM811 and Y₂O₃-modified NCM811 samples.

Table 1. Rietveld refinement parameters of bare and Y₂O₃-coated NCM811 samples.

Sample	a (Å)	c (Å)	c/a	V (Å ³)	R _p (%)	I (003)/I (104)
NCM811	2.8709	14.2044	4.9477	101.4	3.95	1.5066
NCM811@YO400	2.8715	14.2042	4.9466	101.4	4.45	1.5506
NCM811@YO700	2.8740	14.2116	4.9449	101.7	4.01	1.5123
NCM811@YO750	2.8748	14.2136	4.9442	101.7	4.23	1.5263

The scanning electron microscope image is shown in Figure 2a–d. Through the observation of NCM811, the sample presents a similar spherical appearance, and the diameter of the particles is between 10 and 15 μm . The particles are composed of original particles with smaller particle size [35]. The enlarged SEM image is shown in Figure 2a1–d1. The surface of the original sample is relatively smooth, while the surface of the Y_2O_3 sample coated at 400 $^\circ\text{C}$ is rough. This may be due to the coating effect of Y_2O_3 on the surface of the bare NCM811 sample. The surface of the modified sample is smooth at 700 $^\circ\text{C}$ and 750 $^\circ\text{C}$. Compared with NCM811 particles without Y_2O_3 modification, the particles of the modified samples are denser. The reduction in voids may be due to the diffusion of Y_2O_3 coating into the particle voids at high temperatures, which is more beneficial for reducing the chances of electrolytes entering the gaps and then restraining the harmful reaction. The surface of NCM@YO700 was analyzed using an EDS test to further understand the elemental distribution of the coating. The main element components Ni, Co, and Mn are uniformly distributed on the surface of the sample [36], as shown in Figure 2e–g. In addition, Y can be observed in Figure 2h, which reaffirms the success of the Y_2O_3 coating in the NCM811 sample.

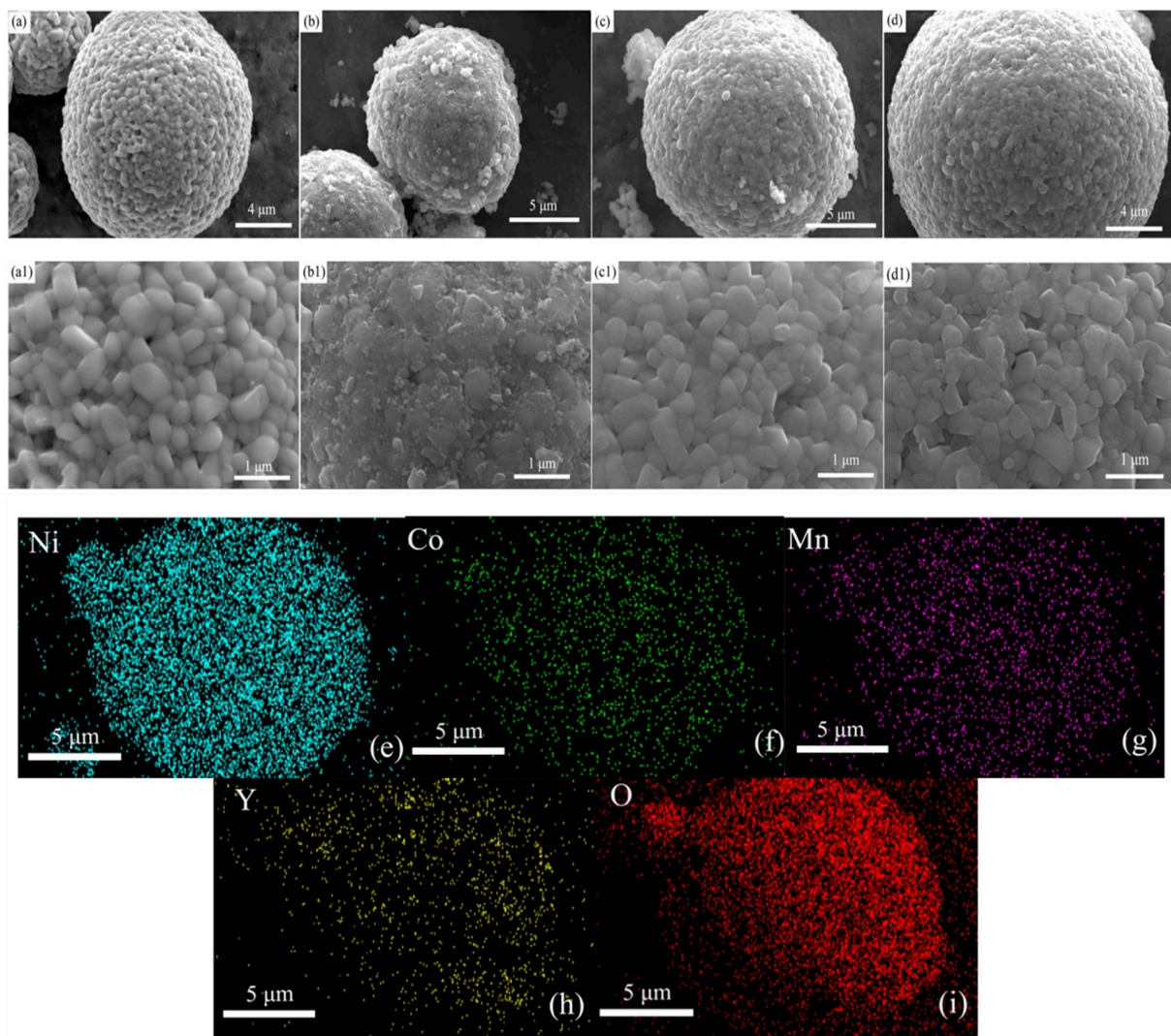


Figure 2. SEM images of pure NCM811 and Y_2O_3 -modified NCM811 materials; (a) NCM811; (b) NCM@YO400; (c) NCM@YO700; (d) NCM@YO750; (a1–d1) the enlarged images of (a–i) EDS mappings of NCM@YO700.

The transmission electron microscope images in Figure 3 show the crystal structure of NCM811 and NCM@YO700 samples, with continuous and straight lattice stripes, indicating high crystallinity and good layered structure. In Figure 3a, the spacings of the (003), (006), and (101) planes of the NCM sample are 0.476 nm, 0.237 nm, and 0.245 nm, respectively. Figure 3b shows that Y_2O_3 successfully coats the surface of the substrate, and the composition analysis of the coating is carried out. In Figure 3c, the (003) plane spacing of the NCM-@YO700 sample is 0.481 nm. The crystal plane spacing of NCM-@YO700 is slightly wider than bare NCM811 [37]. It is proved that a certain amount of Y enters the lattice of NCM811. Since the ionic radius of the transition metal ion M (M = Ni, Co, Mn) is smaller than Y^{3+} , the sample lattice spacing increases, and the cell volume of the sample increases, which is consistent with the results analyzed with the X-ray diffractometer. The magnification analysis of Figure 3I,II shows that the distance between crystal planes is 0.251 nm, 0.209 nm, and 0.160 nm, corresponding to (411), (134), and (622) of Y_2O_3 , respectively, indicating that some Y_2O_3 coating is realized on the surface of the NCM811 samples to some extent.

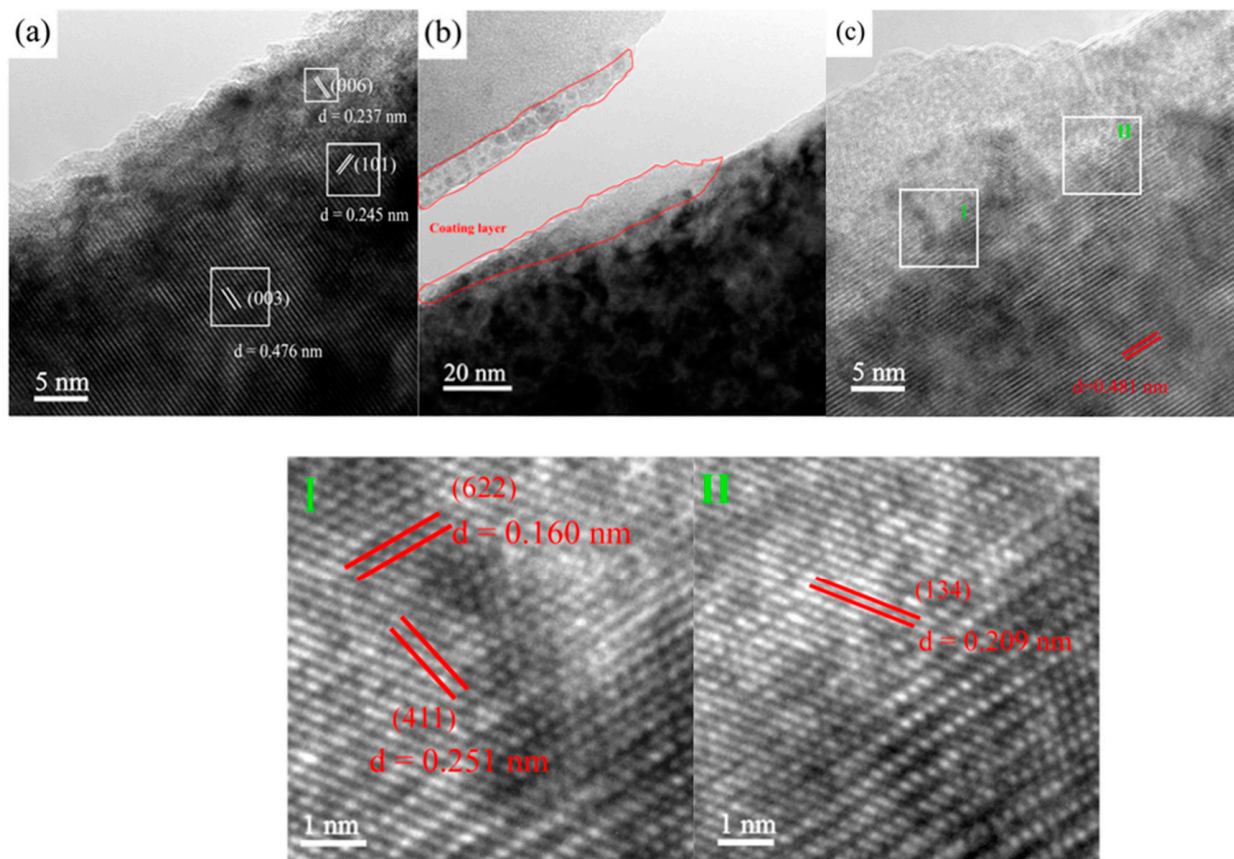


Figure 3. HRTEM images of the bare NCM811 and NCM@YO700; (a) bare NCM811; (b,c) NCM@YO700; and (I,II) the enlarged images of (c).

The XPS analysis of the surface elements of the materials reveals important information about their oxidation valence states. In Figure 4a, Ni $2p_{3/2}$ and $2p_{1/2}$ exhibit two peaks at 854.8 eV and 872.2 eV [38,39]. The Ni $2p_{3/2}$ spectrum shows deconvolution peaks at 854.6 eV and 855.7 eV, indicating the presence of Ni^{2+} and Ni^{3+} valence states. According to Figure 4b,c, the Co $2p_{1/2}$ and Mn $2p_{1/2}$ peaks are observed at 794.9 eV and 654.2 eV, respectively. The Co $2p_{3/2}$ and Mn $2p_{3/2}$ peaks are observed at 780.0 eV and 642.6 eV, respectively. This indicates that the valence states of Co and Mn are mainly trivalent and tetravalent [40]. In Figure 4d, the decrease in lithium peak intensity may be attributed to the Y_2O_3 modification. The O 1s peak at 529.4 eV is related to the lattice oxygen in the

metal skeleton in Figure 4e. The intensity of the lattice oxygen peaks is enhanced compared to the untreated Y_2O_3 samples. Similar conclusions have been previously reported in the literature [38,41]. This enhancement indicates an increase in oxygen vacancy peak area, which effectively inhibits the loss of oxygen and improves the structural stability of the material [42]. As shown in Figure 4f, the binding energies for Y $2p_{5/2}$ and Y $2p_{3/2}$ of the modified samples are measured at 156.48 eV and 158.48 eV, respectively, indicating that the valence state of Y is +3.

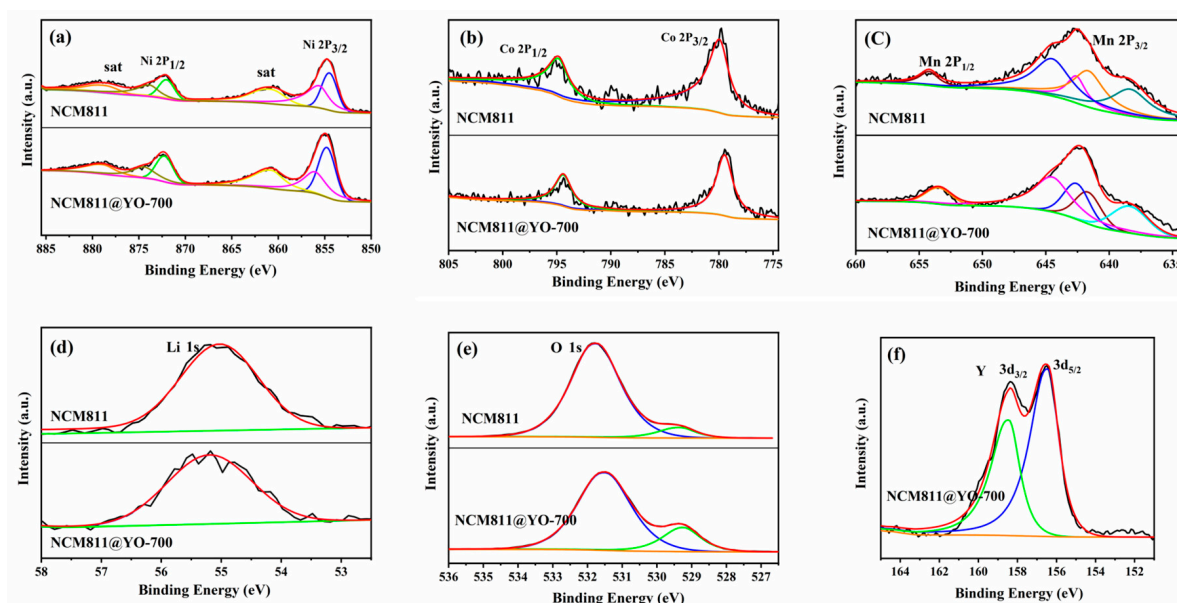


Figure 4. (a–e) XPS data and the fitting results of Ni, Co, Mn, Li, and O of the NCM811 and NCM@YO700 samples; (f) XPS spectra of Y for NCM@YO700.

Figure 5a shows the charge and discharge data of NCM811, NCM811@YO400, NCM811@YO700, and NCM811@YO750 at a sub-constant current of 0.2 C (1 C = 200 mA g^{-1}) and room temperature. The naked NCM811 and the Y_2O_3 -coated sample have a similar discharge platform. At the current density of 0.2 C, the discharge capacities of NCM811, NCM811@YO400, NCM811@YO700, and NCM811@YO750 are measured to be 189.4 mAh g^{-1} , 198.1 mAh g^{-1} , 201.9 mAh g^{-1} , and 203.1 mAh g^{-1} , respectively. Y_2O_3 coating improves the specific discharge capacity of NCM811. At higher sintering temperatures of 700 °C and 750 °C, the discharge capacity increases more obviously since some Y_2O_3 diffuses into the gap of the primary intergranular pores of NCM811 against electrolyte attack, and other Y_2O_3 is doped into the layered structure of NCM811, thereby enlarging the Li^+ ion transport channels. The dual effect of coating and doping is realized through Y_2O_3 modification, leading to the enhanced discharge capacity and improved electrochemical performance of the material. Figure 5b presents the cycling performance of the samples at 1 C and the corresponding electrochemical parameters are shown in Table 2. The capacity of NCM811@YO700 after 150 cycles is measured to be 183.6 mAh g^{-1} , and the retention efficiency is 96.58%. This improvement in cycling stability can be attributed to the role of Y doping in stabilizing the crystal structure of NCM811 and enhancing its stability. Additionally, a portion of Y remains on the surface of NCM811, which helps resist electrolyte erosion and improve electrochemical stability. The rate performance of NCM811 and Y_2O_3 -coated samples is tested in the voltage range of 2.7 V–4.3 V at room temperature, as depicted in Figure 5c. At 5 C, the discharge capacity of NCM811 and NCM811@YO700 is measured to be 107.54 mAh g^{-1} and 138.88 mAh g^{-1} , respectively, indicating a significant improvement in rate performance. This can be attributed to the effective inhibition of harmful reactions between the electrolyte and active substances through the Y_2O_3 coating. Figure 5d shows the cycling data of the samples at 2.7 V–4.5 V, which follows a similar

trend to Figure 5b. After modification with Y_2O_3 , NCM811@YO700 exhibits a capacity of $147.20 \text{ mAh g}^{-1}$ and a retention efficiency of 76.44% after 150 cycles. The coating of Y_2O_3 can also effectively reduce the capacity attenuation. However, for the same sample, the cyclic attenuation at 4.5 V is significantly worse than that at 4.3 V. Under the condition of deep lithium removal at high potential, Ni^{3+} and O^{2-} in high-nickel ternary cathode materials oxidize at the same time to form Ni^{3+} and highly active oxygen [O] (such as O^- , O^{2-}). The electrolyte irreversibly reacts with it to produce gas, which is not conducive to surface charge transfer, resulting in fast capacity decay [41,43].

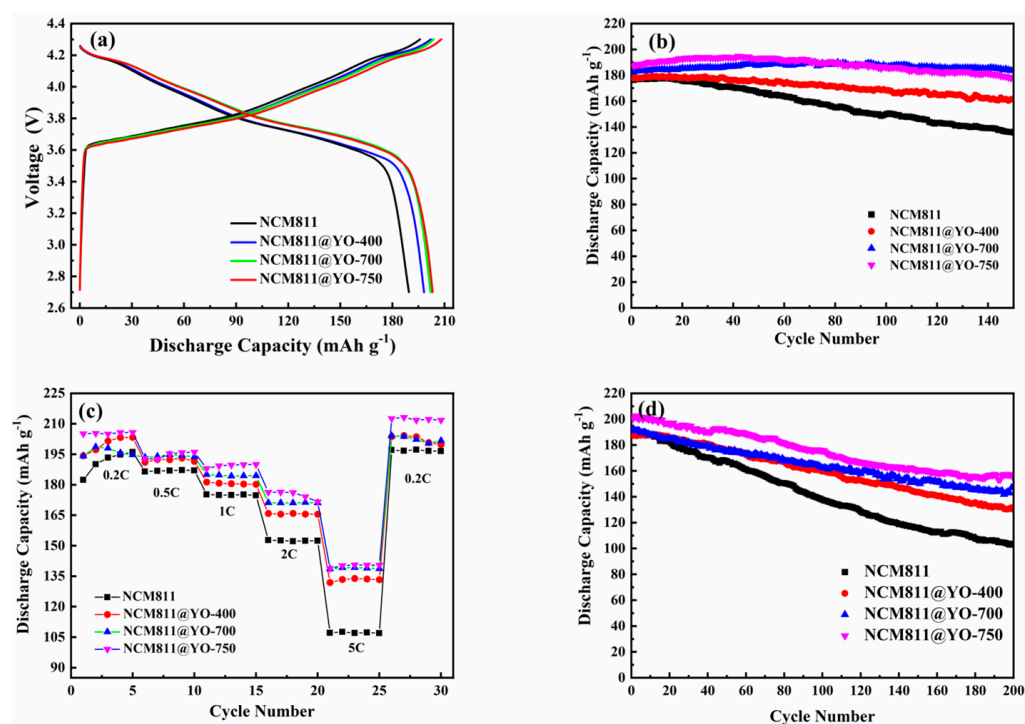


Figure 5. (a) Charge and discharge curves for NCM811 and NCM@YO400, NCM@YO700, and NCM@YO750 in the range of 2.7–4.3 V at 0.2 C. (b) Cycling performance for the NCM811 and NCM811@YO samples at 1 C for 150 cycles. (c) Specific capacity of NCM811 and NCM811@YO samples at different multipliers from 0.2 C to 5 C. (d) Cycling performance of NCM811 and NCM811@YO at 1 C over the high voltage range of 2.7–4.5 V.

Table 2. Electrochemical performance of the pristine and Y_2O_3 -modified samples in the range of 2.7–4.3 V.

Systems	1st Discharge Capacity (mAh g ⁻¹)	Maximum Discharge Capacity (mAh g ⁻¹)	150 st Discharge Capacity (mAh g ⁻¹)	Capacity Retention (%)
Original	176.3	177.9	135.7	76.28
NCM811@YO400	177.7	179.3	161.5	90.07
NCM811@YO700	182.9	190.1	183.6	96.58
NCM811@YO750	187.3	194.7	177.8	91.32

In order to further confirm the results, the SEM analyses of NCM811 and NCM@YO700 after 200 cycles were conducted in Figure 6. Obvious microcracks can be observed in the particles of bare NCM811 after cycling in Figure 6a1. The morphology of the NCM@YO700 particles remains relatively intact in Figure 6b1, and there are no obvious microcracks. It can be demonstrated that coating Y_2O_3 on the surface of particles can result in decreased electrolyte corrosion, preserved crystal structure stability, and ultimately improved material properties. This inference is similar to the explanation reported by Du et al. [44].

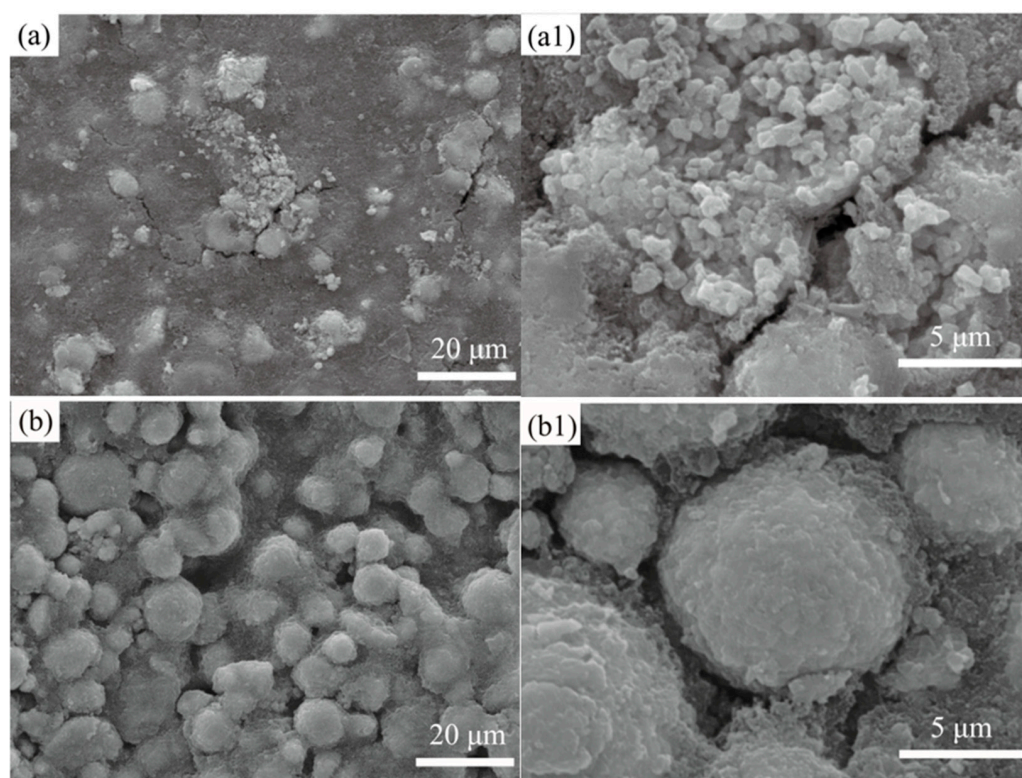


Figure 6. SEM images of NCM811 and Y_2O_3 -modified NCM811 samples after 200 charge/discharge cycles; (a) bare NCM811; (b) NCM@YO700; and (a1,b1) the enlarged images of (a,b).

To further understand the electrochemical performance of the electrode, cyclic voltammetry (CV) tests were carried out, as shown in Figure 7a,b. The CV curves of the NCM811 and NCM811@YO700 samples are similar. It shows that there is no significant change in the electrochemical reaction in the case of Y_2O_3 -coated NCM811. In the second cycle, two redox peaks are observed for NCM811, with the lower peak at 3.945 V/3.624 V corresponding to Ni^{2+}/Ni^{3+} and the higher peak at 4.265 V/4.097 V corresponding to Ni^{3+}/Ni^{4+} . For NCM811@YO700, the redox peak is observed at 3.859 V/3.653 V and 4.253 V/4.128 V. The difference of potential difference ΔE becomes smaller during circulation. The decrease in the potential difference between the anodic and cathodic peaks in NCM811@YO700 (0.47 V) compared to NCM811 (0.66 V) indicates that the Y_2O_3 coating effectively reduces the polarization of the original sample. This reduction in polarization can lead to improved electrochemical kinetics and enhanced overall performance of the material [45]. In addition, compared with the exposed NCM811, NCM811@YO700 shows highly overlapping reduction peaks in the first three cycles, indicating that NCM811@YO700 has a smaller irreversible capacity.

The electrochemical impedance spectra (EIS) of the original NCM811 and NCM811@YO700 were analyzed to investigate the electrochemical kinetic properties. The EIS measurements were conducted after 150 charge–discharge cycles, as shown in Figure 7c, and the equivalent circuit fitting results were obtained with Z-View software. The EIS consists of a concave semicircle and a diagonal line. At high frequency, the intercept with the semicircular x-axis corresponds to the total resistance (R_s), which includes contact resistance, material resistance, and electrolyte ohmic resistance. The R_{sf} and R_{ct} represent the resistance at the electrode–electrolyte interface and the resistance associated with charge transfer processes, respectively. The Warburg impedance (Z_w) is a characteristic impedance resulting from the diffusion limitation of ions. At low frequencies, the EIS can be represented by a diagonal line; the non-ideal capacitance of the surface layer is represented by a constant phase angle element (CPE) [32,46]. The values of NCM811 and NCM811@YO700 are calculated with the given equivalent circuit. For NCM811 and the coated samples, R_{sf} is much smaller

than R_{ct} , which indicates that R_{ct} is the main factor affecting the electrochemical reaction (Seen in Table 3 for details). The R_{ct} value of NCM811@YO700 is smaller than the bare NCM811, which indicates that the coating of Y_2O_3 improves the conductivity of lithium ions. Similar results have appeared in previous studies [46,47]. The Li^+ ion diffusion coefficient is estimated by the following formula [48].

$$D_{Li^+} = \frac{R^2 T^2}{2A^2 n^2 F^2 C^2 \sigma^2} \quad (1)$$

Table 3. Fitted values of impedance parameters of NCM811 and NCM811@YO700.

Electrode	R_s (Ω)	R_{sf} (Ω)	R_{ct} (Ω)	D_{Li^+} ($cm^2 s^{-1}$)
NCM811	14.5	179.6	535.1	1.12×10^{-14}
NCM811@YO700	9.5	85.3	322.8	2.28×10^{-14}

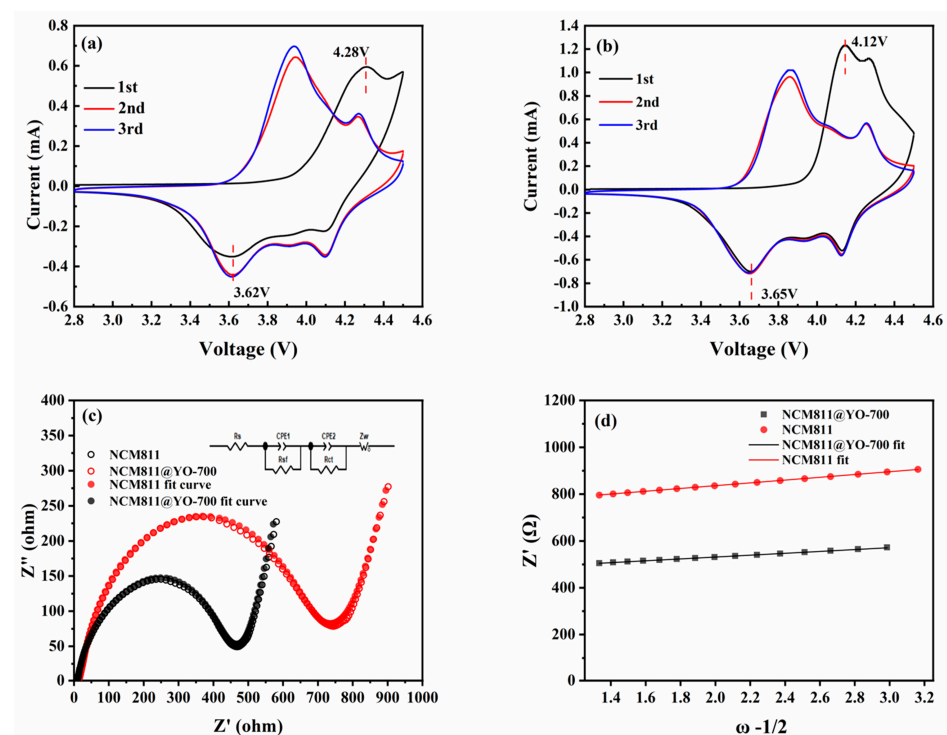


Figure 7. The CV curves in the voltage range of 2.8–4.3 V for (a) NCM811 and (b) NCM811@YO700. (c) The EIS and equivalent circuit-fitted graph after 150 charge/discharge cycles. (d) The relationship between Z' and $\omega^{-1/2}$.

The gas constant ($8.314 \text{ J K}^{-1} \text{ mol}^{-1}$), the absolute temperature (298 K), the electrode's surface (1.654 cm^2), the number of electrons involved in the reaction ($n = 1$), the Faraday constant, and the Warburg coefficient are represented by the variables R , T , A , n , F , and σ , respectively [49]. C in this study is $0.00718 \text{ mol cm}^{-3}$, which is the concentration of lithium ions. The value of σ can be obtained by linearly fitting the slope of Z' to the frequency $\omega^{-1/2}$ (Figure 7d). The D_{Li^+} value of NCM811 increases from $1.12 \times 10^{-14} \text{ cm}^2 \text{ S}^{-1}$ to $2.28 \times 10^{-14} \text{ cm}^2 \text{ S}^{-1}$ after Y_2O_3 modification. Considering that NCM811 and NCM811@YO700 have similar structures and particle sizes, the enhancement of Li^+ ion mobility can be attributed to the Y_2O_3 coating on the NCM811 interface. There have been similar reports previously [32,50,51].

4. Conclusions

Y₂O₃-modified NCM811 samples were made by dry milling and heat treating at sintering temperatures of 400 °C, 700 °C, and 750 °C in order to enhance the electrochemical performance of NCM811. The discharge capacity, rate performance, and cycle stability are all significantly enhanced by the Y₂O₃ alteration. Particularly, the NCM811@YO700 (sintered at 700 °C) demonstrates excellent cyclic stability with a capacity retention efficiency of 96.58% after 150 cycles at 2.7 V–4.3 V, which is much higher than the 76.28% of the bare NCM811, and still retains the discharge capacity of 183.6 mAh g⁻¹ after cycling. Also, the rate capacity is greatly enhanced at high current density for Y₂O₃-modified NCM811. The discharge capacity of NCM811 and NCM811@YO700 is 107.54 mAh g⁻¹ and 138.88 mAh g⁻¹ at 5 C. The results show that dual coating and doping effects can be achieved through Y₂O₃ modification. Y₂O₃ coating can reduce the direct contact between the surface of NCM811 and the electrolyte, which is conducive to the inhibition of interfacial side reactions and the enhancement of electrochemical reactions. The other portion of Y diffuses into the layer structure, which can stabilize the crystal structure, promote lithium-ion transport, and enhance the cycling performance. The Y₂O₃ dry milling method makes them have great application potential as high-energy-density cathode material.

Supplementary Materials: The following supporting information can be downloaded at <https://www.mdpi.com/article/10.3390/coatings14040443/s1>: Figure S1: The positive electrode materials used in the experiment were pure NCM811 and Y₂O₃-modified NCM811 samples, (a) bare NCM811, (b) NCM@YO400, (c) NCM@YO700, (d) NCM@YO750.; Figure S2: Pictures of CR2032 button half-coin batteries in this experiment.

Author Contributions: Conceptualization, J.W., F.W. and X.W.; methodology, validation, X.W. and M.Z.; formal analysis, J.D., P.L., D.L. and X.W.; investigation, X.W. and M.Z.; writing—original draft preparation, X.W.; writing—review and editing, F.W., M.R. and J.W.; project administration, J.D., M.R., P.L. and D.L.; funding acquisition, M.R. All authors have read and agreed to the published version of the manuscript.

Funding: This research was funded by the National Natural Science Foundation of China (grant numbers 52261003 and 52361037), the Guangxi Key Laboratory of Information Materials and the Guilin University of Electronic Technology, China (221023-Z), and the Innovation Project of GUET Graduate Education (2023 YCXS153).

Institutional Review Board Statement: Not applicable.

Informed Consent Statement: Not applicable.

Data Availability Statement: Data are contained within the article and Supplementary Materials.

Conflicts of Interest: The authors declare no conflicts of interest.

References

1. Li, X.; Han, X.; Li, G.; Du, J.; Cao, Y.; Gong, H.; Wang, H.; Zhang, Y.; Liu, S.; Zhang, B.; et al. Nonsacrificial Nitrile Additive for Armoring High-Voltage LiNi_(0.83)Co_(0.07)Mn_(0.1)O₍₂₎ Cathode with Reliable Electrode-Electrolyte Interface toward Durable Battery. *Small* **2022**, *18*, e2202989. [CrossRef]
2. Yee, M.; An, K.; Nguyen, D.-T.; Yun, H.W.; Park, J.; Suk, J.; Song, S.-W. Confining nonflammable liquid in solid polymer electrolyte to enable nickel-rich cathode-based 4.2 V high-energy solid-state lithium-metal and lithium-ion batteries. *Mater. Today Energy* **2022**, *24*, 100950. [CrossRef]
3. Xu, G.L.; Liu, X.; Daali, A.; Amine, R.; Chen, Z.; Amine, K. Challenges and Strategies to Advance High-Energy Nickel-Rich Layered Lithium Transition Metal Oxide Cathodes for Harsh Operation. *Adv. Funct. Mater.* **2020**, *30*, 2004748. [CrossRef]
4. Goodenough, J.B.; Kim, Y. Challenges for Rechargeable Li Batteries. *Chem. Mater.* **2009**, *22*, 587–603. [CrossRef]
5. Zhai, Y.; Zhang, J.; Zhao, H.; Hu, Z.; Liu, X. Research progress of ternary layered oxide cathode materials for lithium ion batteries. *J. Eng. Stud.* **2017**, *9*, 523. [CrossRef]
6. Zhao, R.; Liang, J.; Huang, J.; Zeng, R.; Zhang, J.; Chen, H.; Shi, G. Improving the Ni-rich LiNi_{0.5}Co_{0.2}Mn_{0.3}O₂ cathode properties at high operating voltage by double coating layer of Al₂O₃ and AlPO₄. *J. Alloys Compd.* **2017**, *724*, 1109–1116. [CrossRef]
7. Li, J.; Xiang, J.; Yi, G.; Tang, Y.; Shao, H.; Liu, X.; Shan, B.; Chen, R. Reduction of Surface Residual Lithium Compounds for Single-Crystal LiNi_{0.6}Mn_{0.2}Co_{0.2}O₂ via Al₂O₃ Atomic Layer Deposition and Post-Annealing. *Coatings* **2022**, *12*, 84. [CrossRef]

8. Bian, X.; Fu, Q.; Bie, X.; Yang, P.; Qiu, H.; Pang, Q.; Chen, G.; Du, F.; Wei, Y. Improved electrochemical performance and thermal stability of Li-excess $\text{Li}_{1.18}\text{Co}_{0.15}\text{Ni}_{0.15}\text{Mn}_{0.52}\text{O}_2$ cathode material by Li_3PO_4 surface coating. *Electrochim. Acta* **2015**, *174*, 875–884. [[CrossRef](#)]
9. Ma, F.; Wu, Y.; Wei, G.; Qiu, S.; Qu, J. Enhanced electrochemical performance of $\text{LiNi}_{0.8}\text{Co}_{0.1}\text{Mn}_{0.1}\text{O}_2$ cathode via wet-chemical coating of MgO. *J. Solid State Electrochem.* **2019**, *23*, 2213–2224. [[CrossRef](#)]
10. Yu, Z.; Tong, Q.; Zhao, G.; Zhu, G.; Tian, B.; Cheng, Y. Combining Surface Holistic Ge Coating and Subsurface Mg Doping to Enhance the Electrochemical Performance of $\text{LiNi}_{0.8}\text{Co}_{0.1}\text{Mn}_{0.1}\text{O}_2$ Cathodes. *ACS Appl. Mater. Interfaces* **2022**, *14*, 25490–25500. [[CrossRef](#)]
11. Feng, Y.; Zhang, X.; Lin, C.; Wang, Q.; Zhang, Y. Improving the electrochemical performance of $\text{LiNi}_{0.8}\text{Co}_{0.1}\text{Mn}_{0.1}\text{O}_2$ cathodes using a simple Ce^{4+} -doping and CeO_2 -coating technique. *N. J. Chem.* **2021**, *45*, 21617–21623. [[CrossRef](#)]
12. Li, D.; Guo, H.; Jiang, S.; Zeng, G.; Zhou, W.; Li, Z. Microstructures and electrochemical performances of TiO_2 -coated Mg–Zr co-doped NCM as a cathode material for lithium-ion batteries with high power and long circular life. *N. J. Chem.* **2021**, *45*, 19446–19455. [[CrossRef](#)]
13. Tang, W.; Peng, Z.; Shi, Y.; Xu, S.; Shuai, H.; Zhou, S.; Kong, Y.; Yan, K.; Lu, T.; Wang, G. Enhanced cyclability and safety performance of $\text{LiNi}_{0.6}\text{Co}_{0.2}\text{Mn}_{0.2}\text{O}_2$ at elevated temperature by AlPO_4 modification. *J. Alloys Compd.* **2019**, *810*, 151834. [[CrossRef](#)]
14. Yang, C.; Li, Y.; Zhang, X.; Xiao, J.; Xiong, H.; Li, W.; Guo, P.; Yang, Z.; Xie, M. Enhanced cyclic stability of $\text{LiNi}_{0.8}\text{Co}_{0.1}\text{Mn}_{0.1}\text{O}_2$ (NCM811) by AlF_3 coating via atomic layer deposition. *Ionics* **2022**, *28*, 4547–4554. [[CrossRef](#)]
15. Li, M.; Wang, H.; Zhao, L.; Zhang, F.; He, D. The combined effect of CaF_2 and graphite two-layer coatings on improving the electrochemical performance of Li-rich layer oxide material. *J. Solid State Chem.* **2019**, *272*, 38–46. [[CrossRef](#)]
16. Zhou, S.; Zhang, X.; Zhang, Z.; Liu, S.; Wang, R. Improving the Electrochemical Performance of $\text{LiNi}_{1/3}\text{Co}_{1/3}\text{Mn}_{1/3}\text{O}_2$ Cathode Material by LiF Modification. *Coatings* **2023**, *13*, 727. [[CrossRef](#)]
17. Dai, S.; Yan, G.; Wang, L.; Luo, L.; Li, Y.; Yang, Y.; Liu, H.; Liu, Y.; Yuan, M. Enhanced electrochemical performance and thermal properties of Ni-rich $\text{LiNi}_{0.8}\text{Co}_{0.1}\text{Mn}_{0.1}\text{O}_2$ cathode material via CaF_2 coating. *J. Electroanal. Chem.* **2019**, *847*, 113197. [[CrossRef](#)]
18. Dong, H.; Xie, M.; Cai, M.; Liu, H.; Zhang, Z.; Ye, B.; Zhao, P.; Dong, W.; Huang, F. Amorphous fluorine glaze for crack-free nickel-rich layered cathode grains under electrochemical cycling. *Chem. Eng. J.* **2022**, *436*, 135227. [[CrossRef](#)]
19. Breddemann, U.; Krossing, I. Review on Synthesis, Characterization, and Electrochemical Properties of Fluorinated Nickel-Cobalt-Manganese Cathode Active Materials for Lithium-Ion Batteries. *ChemElectroChem* **2020**, *7*, 1389–1430. [[CrossRef](#)]
20. Yang, S.; Meng, T.; Wang, Z.; Hu, X. Unveiling decaying mechanism of non-flammable all-fluorinated carbonate electrolytes in lithium metal batteries with 4.6-V LiCoO_2 cathodes at elevated temperatures. *Energy Storage Mater.* **2024**, *65*, 103177. [[CrossRef](#)]
21. Ren, Q.; Yuan, Y.; Wang, S. Interfacial Strategies for Suppression of Mn Dissolution in Rechargeable Battery Cathode Materials. *ACS Appl. Mater. Interfaces* **2021**, *14*, 23022–23032. [[CrossRef](#)]
22. Zhang, W.; Tang, X.; Xiao, L.; Xiao, Z. Influence of Al^{3+} and PO_4^{3-} co-doping on structure and electrochemical performance of $\text{LiNi}_{0.8}\text{Co}_{0.1}\text{Mn}_{0.1}\text{O}_2$ cathode materials. *J. Solid State Electrochem.* **2023**, *27*, 1185–1194. [[CrossRef](#)]
23. Li, Y.; Wang, Z.-T.; Liu, G.; Wang, J.; Wang, J. Boosting the electrochemical performance of $\text{LiNi}_{0.8}\text{Co}_{0.1}\text{Mn}_{0.1}\text{O}_2$ cathode materials with $\text{Zn}_3(\text{PO}_4)_2$ surface coating. *Adv. Powder Technol.* **2021**, *32*, 4651–4657. [[CrossRef](#)]
24. Liu, L.; Li, M.; Chu, L.; Jiang, B.; Lin, R.; Zhu, X.; Cao, G. Layered ternary metal oxides: Performance degradation mechanisms as cathodes, and design strategies for high-performance batteries. *Prog. Mater. Sci.* **2020**, *111*, 100655. [[CrossRef](#)]
25. Zhang, X.; Gao, S.; Gui, W.; Zeng, Q. First-principles study of structure, mechanical and optical properties of La- and Sc-doped Y_2O_3 . *J. Rare Earths* **2019**, *37*, 879–885. [[CrossRef](#)]
26. Liu, X.-H.; Kou, L.-Q.; Shi, T.; Liu, K.; Chen, L. Excellent high rate capability and high voltage cycling stability of Y_2O_3 -coated $\text{LiNi}_{0.5}\text{Co}_{0.2}\text{Mn}_{0.3}\text{O}_2$. *J. Power Sources* **2014**, *267*, 874–880. [[CrossRef](#)]
27. Zou, P.; Lin, Z.; Fan, M.; Wang, F.; Liu, Y.; Xiong, X. Facile and efficient fabrication of Li_3PO_4 -coated Ni-rich cathode for high-performance lithium-ion battery. *Appl. Surf. Sci.* **2020**, *504*, 144506. [[CrossRef](#)]
28. Jo, C.-H.; Cho, D.-H.; Noh, H.-J.; Yashiro, H.; Sun, Y.-K.; Myung, S.T. An effective method to reduce residual lithium compounds on Ni-rich $\text{Li}[\text{Ni}_{0.6}\text{Co}_{0.2}\text{Mn}_{0.2}]\text{O}_2$ active material using a phosphoric acid derived Li_3PO_4 nanolayer. *Nano Res.* **2014**, *8*, 1464–1479. [[CrossRef](#)]
29. Kitsche, D.; Tang, Y.; Ma, Y.; Goonetilleke, D.; Sann, J.; Walther, F.; Bianchini, M.; Janek, J.; Brezesinski, T. High Performance All-Solid-State Batteries with a Ni-Rich NCM Cathode Coated by Atomic Layer Deposition and Lithium Thiophosphate Solid Electrolyte. *ACS Appl. Energy Mater.* **2021**, *4*, 7338–7345. [[CrossRef](#)]
30. Wang, X.; Yushin, G. Chemical vapor deposition and atomic layer deposition for advanced lithium ion batteries and supercapacitors. *Energy Environ. Sci.* **2015**, *8*, 1889–1904. [[CrossRef](#)]
31. Nisar, U.; Muralidharan, N.; Essehli, R.; Amin, R.; Belharouak, I. Valuation of Surface Coatings in High-Energy Density Lithium-ion Battery Cathode Materials. *Energy Storage Mater.* **2021**, *38*, 309–328. [[CrossRef](#)]
32. Wang, F.; Luo, Y.; Liu, P.; Balogun, M.-S.; Deng, J.; Wang, Z. Improved Cycling Performance and High Rate Capacity of $\text{LiNi}_{0.8}\text{Co}_{0.1}\text{Mn}_{0.1}\text{O}_2$ Cathode Achieved by $\text{Al}(\text{PO}_3)_3$ Modification via Dry Coating Ball Milling. *Coatings* **2022**, *12*, 319. [[CrossRef](#)]
33. Ran, A.; Chen, S.; Cheng, M.; Liang, Z.; Li, B.; Zhou, G.; Kang, F.; Zhang, X.; Wei, G. A single-crystal nickel-rich material as a highly stable cathode for lithium-ion batteries. *J. Mater. Chem. A* **2022**, *10*, 19680–19689. [[CrossRef](#)]

34. Zhang, M.; Lv, M.; Zhang, D.; Yan, Y.; Wang, Y.; Li, J.; Li, Z. Enhanced electrochemical properties of NCM811 cathode material due to synergistic modification with Sm as doping and coating agent. *J. Alloys Compd.* **2022**, *909*, 164712. [[CrossRef](#)]
35. Xu, Y.-D.; Xiang, W.; Wu, Z.-G.; Xu, C.-L.; Li, Y.-C.; Guo, X.-D.; Lv, G.-P.; Peng, X.; Zhong, B.-H. Improving cycling performance and rate capability of Ni-rich $\text{LiNi}_{0.8}\text{Co}_{0.1}\text{Mn}_{0.1}\text{O}_2$ cathode materials by $\text{Li}_4\text{Ti}_5\text{O}_{12}$ coating. *Electrochim. Acta* **2018**, *268*, 358–365. [[CrossRef](#)]
36. Zhao, S.; Zhu, Y.; Qian, Y.; Wang, N.; Zhao, M.; Yao, J.; Xu, Y. Annealing effects of TiO_2 coating on cycling performance of Ni-rich cathode material $\text{LiNi}_{0.8}\text{Co}_{0.1}\text{Mn}_{0.1}\text{O}_2$ for lithium-ion battery. *Mater. Lett.* **2020**, *265*, 127418. [[CrossRef](#)]
37. Chen, S.; He, T.; Su, Y.; Lu, Y.; Bao, L.; Chen, L.; Zhang, Q.; Wang, J.; Chen, R.; Wu, F. Ni-Rich $\text{LiNi}_{(0.8)}\text{Co}_{(0.1)}\text{Mn}_{(0.1)}\text{O}_{(2)}$ Oxide Coated by Dual-Conductive Layers as High Performance Cathode Material for Lithium-Ion Batteries. *ACS Appl. Mater. Interfaces* **2017**, *9*, 29732–29743. [[CrossRef](#)]
38. Zhang, C.; Liu, S.; Su, J.; Chen, C.; Liu, M.; Chen, X.; Wu, J.; Huang, T.; Yu, A. Revealing the role of NH_4VO_3 treatment in Ni-rich cathode materials with improved electrochemical performance for rechargeable lithium-ion batteries. *Nanoscale* **2018**, *10*, 8820–8831. [[CrossRef](#)]
39. Ding, Y.; Deng, B.; Wang, H.; Li, X.; Chen, T.; Yan, X.; Wan, Q.; Qu, M.; Peng, G. Improved electrochemical performances of $\text{LiNi}_{0.6}\text{Co}_{0.2}\text{Mn}_{0.2}\text{O}_2$ cathode material by reducing lithium residues with the coating of Prussian blue. *J. Alloys Compd.* **2019**, *774*, 451–460. [[CrossRef](#)]
40. Li, L.; Zhang, Z.; Fu, S.; Liu, Z. F127-assisted synthesis of $\text{LiNi}_{0.5}\text{Co}_{0.2}\text{Mn}_{0.3}\text{O}_{1.99}\text{F}_{0.01}$ as a high rate and long lifespan cathode material for lithium-ion batteries. *Appl. Surf. Sci.* **2019**, *476*, 1061–1071. [[CrossRef](#)]
41. House, R.A.; Marie, J.-J.; Pérez-Osorio, M.A.; Rees, G.J.; Boivin, E.; Bruce, P.G. The role of O_2 in O-redox cathodes for Li-ion batteries. *Nat. Energy* **2021**, *6*, 781–789. [[CrossRef](#)]
42. He, R.; Bai, X.; Wei, A.; Zhang, L.; Liu, P.; Liu, Z. Y_2O_3 modification on nickel-rich $\text{LiNi}_{0.8}\text{Co}_{0.1}\text{Mn}_{0.1}\text{O}_2$ with improved electrochemical performance in lithium-ion batteries. *J. Rare Earths* **2022**, *40*, 309–317. [[CrossRef](#)]
43. Lin, F.; Markus, I.M.; Nordlund, D.; Weng, T.-C.; Asta, M.D.; Xin, H.L.; Doeff, M.M. Surface reconstruction and chemical evolution of stoichiometric layered cathode materials for lithium-ion batteries. *Nat. Commun.* **2014**, *5*, 1–9. [[CrossRef](#)] [[PubMed](#)]
44. Du, M.; Yang, P.; He, W.; Bie, S.; Zhao, H.; Yin, J.; Zou, Z.; Liu, J. Enhanced high-voltage cycling stability of Ni-rich $\text{LiNi}_{0.8}\text{Co}_{0.1}\text{Mn}_{0.1}\text{O}_2$ cathode coated with $\text{Li}_2\text{O}-2\text{B}_2\text{O}_3$. *J. Alloys Compd.* **2019**, *805*, 991–998. [[CrossRef](#)]
45. Peng, Z.; Li, T.; Zhang, Z.; Du, K.; Hu, G.; Cao, Y. Surface architecture decoration on enhancing properties of $\text{LiNi}_{0.8}\text{Co}_{0.1}\text{Mn}_{0.1}\text{O}_2$ with building bi-phase Li_3PO_4 and AlPO_4 by $\text{Al}(\text{H}_2\text{PO}_4)_3$ treatment. *Electrochim. Acta* **2020**, *338*, 135870. [[CrossRef](#)]
46. Liu, Y.; Wang, Q.; Zhang, Z.; Dou, A.; Pan, J.; Su, M. Investigation the electrochemical performance of layered cathode material $\text{Li}_{1.2}\text{Ni}_{0.2}\text{Mn}_{0.6}\text{O}_2$ coated with $\text{Li}_4\text{Ti}_5\text{O}_{12}$. *Adv. Powder Technol.* **2016**, *27*, 1481–1487. [[CrossRef](#)]
47. Tan, X.; Zhang, M.; Zhang, D.; Yan, Y.; Wang, Y.; Li, Z. Inhibited intracrystalline cracks and enhanced electrochemical properties of NCM811 cathode materials coated by EPS. *Ceram. Int.* **2021**, *47*, 32710–32719. [[CrossRef](#)]
48. Liu, X.; Chen, Q.; Li, Y.; Chen, C.; Zeng, W.; Yuan, M.; Wang, R.; Xiao, S. Synergistic Modification of Magnesium Fluoride/Sodium for Improving the Electrochemical Performances of High-Nickel Ternary (NCM811) Cathode Materials. *J. Electrochem. Soc.* **2019**, *166*, A3480–A3486. [[CrossRef](#)]
49. Zhao, M.; Chen, Q. Improving the electrochemical performance of $\text{LiNi}_{0.7}\text{Mn}_{0.3}\text{O}_2$ cathode material by CeO_2 coating via Ce doping. *Solid State Ion.* **2023**, *399*, 116296. [[CrossRef](#)]
50. Wu, Y.S.; Pham, Q.-T.; Yang, C.-C.; Chern, C.-S.; Babulal, L.M.; Seenivasan, M.; Jeyakumar, J.; Mengesha, T.H.; Placke, T.; Bruncklaus, G.; et al. Coating of a Novel Lithium-Containing Hybrid Oligomer Additive on Nickel-Rich $\text{LiNi}_{0.8}\text{Co}_{0.1}\text{Mn}_{0.1}\text{O}_2$ Cathode Materials for High-Stability and High-Safety Lithium-Ion Batteries. *ACS Sustain. Chem. Eng.* **2022**, *10*, 7394–7408. [[CrossRef](#)]
51. Cheng, W.; Li, L.; Hao, S.; Liu, L.; Wu, Y.; Huo, J.; Ji, Y.; Liu, X. Face-lifting the surface of $\text{LiNi}_{0.8}\text{Co}_{0.15}\text{Al}_{0.05}\text{O}_2$ cathode via $\text{Y}(\text{PO}_3)_3$ to form an in situ triple composite Li-ion conductor coating layer with the enhanced electrochemical performance. *Nanotechnology* **2022**, *33*, 375701. [[CrossRef](#)]

Disclaimer/Publisher’s Note: The statements, opinions and data contained in all publications are solely those of the individual author(s) and contributor(s) and not of MDPI and/or the editor(s). MDPI and/or the editor(s) disclaim responsibility for any injury to people or property resulting from any ideas, methods, instructions or products referred to in the content.